Title
The effect of permeate flux on membrane fouling during microfiltration of oily water

Authors
He, Zhengwang
Miller, Daniel J
Kasemset, Sirirat
et al.

Publication Date
2017-03-01

DOI
10.1016/j.memsci.2016.10.002

Peer reviewed

Constant Permeate Flux Microfiltration of Oily Water

Zhengwang He, Daniel J. Miller[1], Sirirat Kasemset[2], Donald R. Paul, Benny D. Freeman*

Department of Chemical Engineering, Center for Energy and Environmental Resources, and Texas Materials Institute, The University of Texas at Austin, 10100 Burnet Road Building 133, Austin, TX 78758

*Corresponding author (Tel: +1-512-232-2803; Email: freeman@che.utexas.edu)

1. Current address: Joint Center for Artificial Photosynthesis, Lawrence Berkeley National Laboratory, 1 Cyclotron Road, Berkeley CA 94702

2. Current address: Evonik Corporation, 4201 Evonik Road, Theodore, AL 36582

Manuscript prepared for submission to *Journal of Membrane Science*

GRAPHICAL ABSTRACT

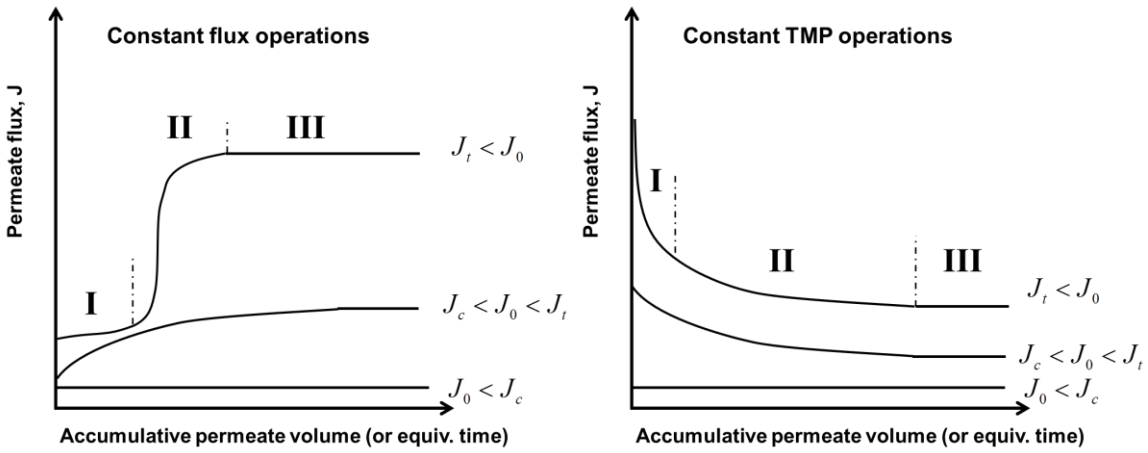

HIGHLIGHTS

1. Critical and threshold fluxes were determined using the flux-stepping technique.
2. Fouling tests were performed below and above the critical and threshold fluxes.
3. Below the threshold flux, resistance was predicted by flux-stepping experiments.
4. Above the threshold flux, critical pressure is the upper limit of TMP.

ABSTRACT

Critical and threshold flux concepts were recently developed to distinguish no fouling, slow fouling and rapid fouling regimes. However, crossflow fouling tests are often performed independent of critical and threshold flux determinations. In this study, a poly(vinylidene) fluoride microfiltration membrane was challenged with various oil-in-water emulsions. The critical and threshold flux values were estimated using the flux-stepping technique. A constant mass transfer resistance below the threshold flux, R_B, was determined from linear regression of flux-stepping results. Constant flux crossflow fouling tests were performed at selected fluxes below and above the critical and threshold fluxes. Below the critical flux, mass transfer resistance remained constant at clean membrane resistance. Below the threshold flux, mass transfer resistance approached a steady state resistance that coincided with R_B values determined from flux-stepping experiments. Above the threshold flux, transmembrane pressure (TMP) presented a three-stage profile, an initial gradual increase stage, a TMP jump stage, and a pseudo-steady stage. The pseudo-steady state TMP corresponded to the critical pressure of an oil layer.

KEYWORDS

Critical flux, threshold flux, constant flux fouling, TMP profile, critical pressure

1. INTRODUCTION

The critical flux concept was introduced by Field et al. in 1995 [1]. Critical flux, J_c, was defined as "on start-up there exists a flux below which a decline of flux with time does not occur; above it fouling is observed" [1]. Realistic operations can hardly achieve a zero fouling scenario as prescribed by the critical flux definition. In 2011, Field and Pearce introduced the threshold flux concept analogous to the critical flux concept, which takes into account realistic operations. Threshold flux, J_t, is defined based on the rate of fouling. Below the threshold flux, the rate of fouling is slow or near constant. Many of the earlier reported critical fluxes are, in fact, threshold fluxes [2]. Membrane processes are recommended to operate below the threshold flux to maintain a sustainable operation. However, most reported fouling tests are performed independent of critical or threshold flux determination. Without the estimated of critical and threshold fluxes, many reported fouling studies were in the rapid fouling regime (i.e., above the threshold flux). Very few studies focused on the slow fouling regime (i.e., below the threshold flux), which is more pertinent to realistic operations.

Ultrafiltration (UF) and microfiltration (MF) are pressure-driven separations. Membrane fouling tests can be performed in one of the two operational modes, the constant transmembrane pressure (TMP) mode or the constant flux mode. Most laboratory fouling tests are operated in constant TMP mode, while most industrial operations are in constant flux mode. The two operations differ in the local hydrodynamic conditions at the membrane surface. Fouling behavior and fouling mechanisms, which largely depend on hydrodynamic conditions, are likely to vary between the two operations. However, direct comparisons of the two operational modes are very limited in the literature. Sim et al. compared fouling index and membrane resistance between

constant TMP and constant flux ultrafiltration processes [3]. Vyas et al. observed the same extent of fouling when the initial flux was below a certain flux among the two operational modes [4]. Miller et al. observed similar fouling behavior below the threshold flux regardless of the operational modes and dissimilar fouling behavior above the threshold flux [5].

This study aims to provide a framework for constant flux fouling studies and to bridge the constant TMP and constant flux operations using the threshold flux concept. A poly(vinylidene) fluoride (PVDF) MF membrane was challenged with various oil-in-water emulsions. Critical and threshold fluxes were estimated using the flux-stepping technique. Constant flux crossflow fouling tests were performed at selected fluxes, below J_c, below J_t, and above J_t. Below J_c, mass transfer resistance was a constant, and it equaled to the clean membrane resistance. Below J_t, membrane resistance approached a steady state resistance predicted by flux-stepping experiments. Moreover, constant TMP and constant flux operations were comparable below J_t. Above J_t, fouling evolves in three stages in constant flux operations. The final pseudo-steady state TMP correlated with the critical pressure of an oil layer.

2. BACKGROUND AND THEORY

2.1 Critical and threshold flux concepts

The critical flux, J_c, concept was first proposed by Field in 1995 to describe a flux below which fouling is negligible [1]. Critical fluxes can take in one of the two forms, a strong form critical flux or a weak form critical flux, depending on whether adsorptive fouling affects mass transfer resistance. Adsorptive fouling is the spontaneous adsorption of foulants on a membrane surface, and it is not flux-driven. The critical flux

is a strong form critical flux if no adsorptive fouling occurs or adsorptive fouling does not affect mass transfer resistance. The weak form critical flux accounts for adsorptive fouling. Threshold flux, J_t, separates the slow fouling regime from the rapid fouling regime.

In laboratory studies, critical and threshold fluxes are typically estimated using a flux-stepping technique. TMP is monitored while the permeate flux is increased stepwise. The critical and threshold flux can be estimated through a linear regression of the average TMP of each flux step, TMP_{avg}, with respect to the imposed flux, as illustrated in Figure 1. Solid blue line is the TMP-flux relationship that corresponds to no fouling (i.e., pure water filtration). Line A is the linear regression of TMP_{avg} below critical flux. In the case of a strong form critical flux, Line A coincides with the solid blue line, such as the one shown in Figure 1, and its equals the clean membrane resistance. In the case of a weak form critical flux, Line A should still intercept the axes at the origin, while its slope equals the sum of clean membrane resistance and the resistance due to adsorption. In cases of severe fouling, a critical flux may be too low to be measured or does not exist. Line B is the linear regression between J_c and J_t. Often overlooked in the literature is that the linearity of Line B indicates a constant resistance at these fluxes. The slope of Line B represent a constant resistance value of R_B. Line C is the linear regression of the first two data points beyond the threshold flux.

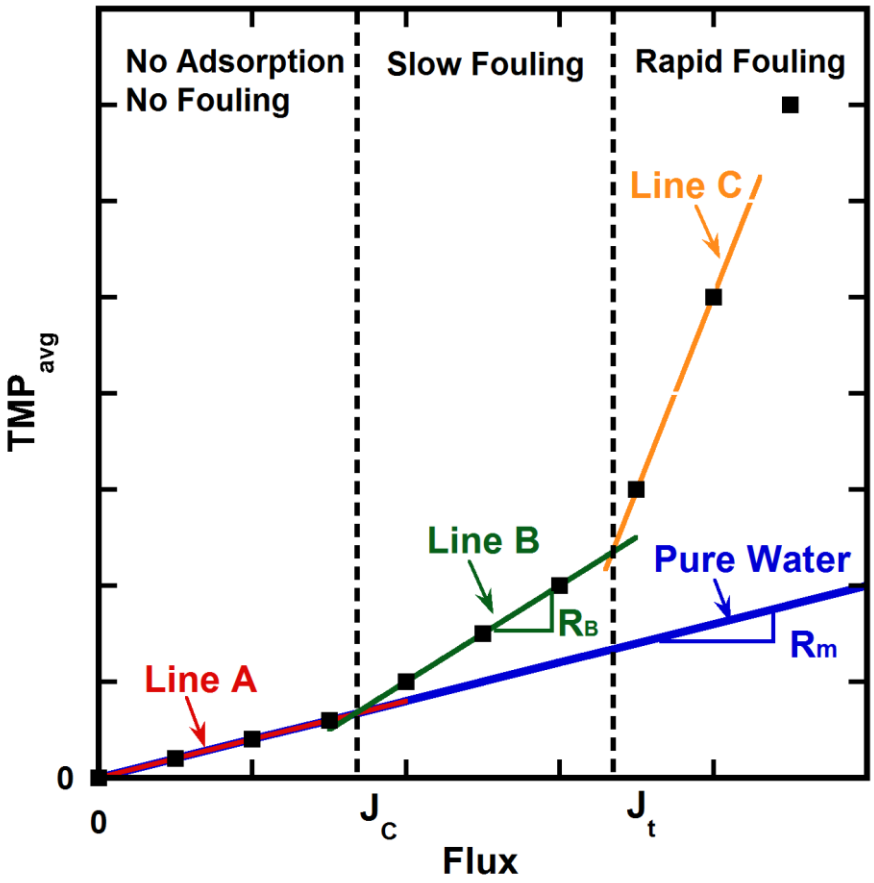

Figure 1. An illustration of critical and threshold flux determination. The solid blue line is TMP-flux for a clean membrane (i.e., pure water filtration). Line A is the linear regression below J_c. Line B is the linear regression between J_c and J_t. Line C is the linear regression of the first two data points beyond J_t. The shown critical flux is a strong form critical flux, so the slope of Line A corresponds to clean membrane resistance. The slope of Line B corresponds to a constant resistance of R_B.

2.2 Constant TMP and constant flux modes

Although most industrial ultrafiltration and microfiltration processes are operated in or very close to the constant flux mode, most laboratory studies are operated in the constant TMP operational mode. The mass transfer resistance, R, is defined as:

$$R = \frac{TMP}{J\mu} \qquad [1]$$

where TMP is the transmembrane pressure, J is the permeate flux, μ is the permeate viscosity. When membranes become fouled during filtration, R increases. In a constant TMP operation, J decreases as R increases, so fouling is often characterized in the form of a declining permeate flux over time. In a constant permeate flux operation, TMP increases as R increases, so fouling is characterized as an increasing TMP over time. To warrant a direct and fair comparison between the two operations, mass transfer resistance should be compared on the basis of cumulative permeate volume per unit membrane area [5]. This allows comparing the extent of fouling when membranes have been be challenged with the same amount of feed and have produced the same amount of permeate.

In a constant TMP operation, the initial flux is always the maximum flux, because the mass transfer resistance is the lowest at the beginning of an experiment. At the membrane surface, the local hydrodynamic conditions vary as permeate flow rate varies with time. On the other hand, in constant flux operations, the overall permeate flow rate is kept constant, so the local hydrodynamics remain the same throughout an experiment. Differences in fouling behavior between the two operations are expected as a result of the differences in local hydrodynamic conditions. Therefore, only operations that started at a similar permeate flux can be directly compared.

2.3 Critical pressure

Typically, ultrafiltration and microfiltration are considered a size sieving process. The selectivity (i.e., sieving coefficient or rejection) depends on the relative size of solutes to membrane pores. Solutes (e.g., particulates, proteins, macromolecules) that are larger than membrane pores are rejected. Emulsified oil droplets differ from rigid particulates or proteins in that they are deformable. Oil droplets can coalesce and breakup into smaller droplets, such that they can enter and penetrate through pores that are apparently smaller than themselves. The deformation of oil droplets at a membrane pore entrance has been investigated by several researchers [6-9]. Nazzal and Wiesner calculated the critical pressure, ΔP_c ,which prevents an oil droplet from entering a membrane pore: [7]

$$\Delta P_c = \frac{4\gamma_{O/W}}{d_p}\left[1-\frac{2+3\cos\theta-\cos^3\theta}{4\left(\frac{d_d}{d_p}\right)^3\cos^3\theta-\left(2-3\sin\theta+\sin^3\theta\right)}\right]^{1/3} \quad [2]$$

where $\gamma_{O/W}$ is the interfacial tension between the oil phase and the aqueous phase, d_d is oil droplet diameter, d_p is membrane pore diameter, and θ is the contact angle between an oil droplet and the membrane surface. If the transmembrane pressure exceeds the critical pressure of an oil droplet, the oil droplet can be deformed to fit in a membrane pore. In crossflow fouling tests, the advancing portion of an oil droplet (i.e., the portion inside the pore) may breakup with the lagging portion (i.e., the portion remains outside the pore), and then permeates through the membrane [8, 9]. When enough oil droplets have deposited on the membrane surface and coalesced to form an oil layer, the critical pressure is the capillary pressure: [ref]

$$\Delta P_c = \frac{4\gamma_{O/W}\cos\theta}{d_p} \quad [3]$$

3. MATERIALS AND METHODS

3.1 Materials

Hydrophobic PVDF MF membranes of 0.2 μm nominal pore rating were generously supplied by Pall Corporation (Port Washington, NY). Flat sheet membrane was received dry. Dry membranes were pretreated by soaking in denatured ethanol for one hour, followed by soaking in ultrapure water for one hour. Membranes were then stored in ultrapure water until further testing. Membrane pure water permeance was 10,000 LMH/bar. Clean membrane resistance was 4×10^9 m^{-1}. The PVDF membrane was hydrophobic, with a water contact angle of 139° [10]. Membrane pore size was characterized with a capillary flow Porometer 3G by Quantachrome Analytical Services (Boynton Beach, Florida). The mean pore diameter was 0.32 μm.

Pennsylvanian grade light crude oil was generously provided by American Refining Group (Bradford, PA). Wesson® soybean oil was purchased from a local supermarket. Sodium chloride of analytical grade and Triton™ X-100 (octylphenol ethylene oxide condensate) non-ionic surfactant were purchased from Sigma Aldrich (St. Louis, MO). Xiameter® OFX-0193, a non-ionic surfactant, was purchased from Dow Corning Corporation (Midland, MI). Denatured ethanol and 1 N sodium hydroxide solution were purchased from Fisher Scientific (Fairlawn, NJ). Ultrapure water (18.2MΩ-cm and 5.4 ppb TOC) was generated by a Millipore (Billerica, MA) RiOS and A10 lab water purification system.

3.2 Model foulant formulation

Soybean and crude oil-in-water emulsions were used as model fouling mixtures. Xiameter and Triton were the surfactant for soybean and crude oil emulsions, respectively. The oil-to-surfactant ratio was 9:1 and 8:2 for soybean and crude oil emulsions, respectively. Typically, a filtration test requires 8 L of oil emulsion. A concentrated oil emulsion was first prepared by blending the oil, surfactant, and ultrapure water (2 L) at 20,000 rpm. Concentrated soybean and crude oil emulsions were blended for 3 and 5 minutes, respectively. To produce the final emulsion, 3 L of ultrapure water was added first, followed by the concentrated emulsion, and then another 3 L of ultrapure water. The final emulsion had a volume of 8 L and a pH of about 5.6. Soybean and crude oil-in-water emulsions had total organic (i.e., oil plus surfactant) concentrations of 200 and 1500 ppm. The oil emulsions were labeled by their oil content. For example, the soybean oil emulsion with a total organic concentration of 1500 ppm is referred to as "soybean 1500".

3.3 Contact angle and interfacial tension measurements

In order to calculate critical pressures of oil droplets and an oil layer (cf., Equations [2] and [3]), contact angle and interfacial tension were measured using a Ramé-Hart Model 200 goniometer (Succasunna, NJ). In both measurements, the aqueous phase was an aqueous solution of surfactants. For example, the soybean 1500 emulsion had a Xiameter concentration of 150 ppm, so the aqueous phase in contact angle and interfacial tension measurements also had 150 ppm of Xiameter.

The contact angle of an oil droplet with respect to the PDVF membrane was measured using a captive bubble method [9]. The PVDF membrane was immersed in the aqueous surfactant solution. A droplet of soybean or crude oil was dispensed and in

contact with the membrane from underneath. The DROPimage software supplied by Ramé-Hart measured the contact angle through the aqueous phase. The interfacial tension between the oil phase and the aqueous phase, $\gamma_{O/W}$, was measured using a pendent drop method. A drop of oil was dispensed by an inverted stainless steel needle immersed in the aqueous phase. The DROPimage software calculated the interfacial tension between the oil drop and the aqueous environment using Laplace-Young equation.

3.4 Crossflow fouling tests

Oil-in-water emulsions were used to challenge a PVDF MF membrane in constant flux crossflow filtration tests. The constant flux crossflow fouling apparatus used in this study has been described in detail elsewhere [10, 11]. The effective filtration area was 19 cm^2. Crossflow feed flow rate was 2 L/min (feed velocity = 43 cm/s, Re $\approx$ 2500). Permeate flux was maintained constant by a peristaltic pump that was in feedback control with a Coriolis flow meter. Three membrane samples were tested simultaneously in each test. Transmembrane pressure is monitored throughout the experiment.

Critical and threshold fluxes were estimated via a flux-stepping technique using the constant flux apparatus. The permeate flux was increased stepwise at 10 LMH ($Lm^{-2}hr^{-1}$) intervals every 15 minutes. Transmembrane pressure throughout the experiment was monitored. Average transmembrane pressure for each step, TMP_{avg}, was analyzed as outlined in Figure 1 to estimate critical and threshold fluxes.

4. RESULTS AND DISCUSSION

4.1 Critical and threshold flux determination

Figure 2 presents TMP_{avg} as a function of the imposed permeate flux. Detailed flux-stepping data is presented in the Supporting Information. Estimated critical and

threshold flux are reported in Table 1. The slope of Line B in TMP_{avg} -flux relationship corresponded to a resistance value, R_B, which is also reported in Table 1. R_B was calculated assuming the permeate viscosity was equal to that of pure water [5, 12]. As discussed in the Supporting Information, the organic content did not affect emulsion viscosity. Results of a polysulfone (PS) ultrafiltration (UF) membrane were adapted from an earlier publication [5].

A strong form critical flux was estimated to be 64 LMH when the PVDF MF membrane was challenged with 200 ppm oil emulsions. For the 1500 ppm oil emulsions, not enough experimental data was available to allow a linear regression that intercepts the axes at the origin. Therefore, a critical flux, a strong form or a weak form, could not be estimated. The critical flux, if exists, should be below 40 LMH. A threshold flux was determined for each oil emulsion, and it can be used to evaluate membrane fouling propensity [10]. The threshold flux decreased with increasing oil concentration, indicating increasing feed concentration increased membrane fouling propensity.

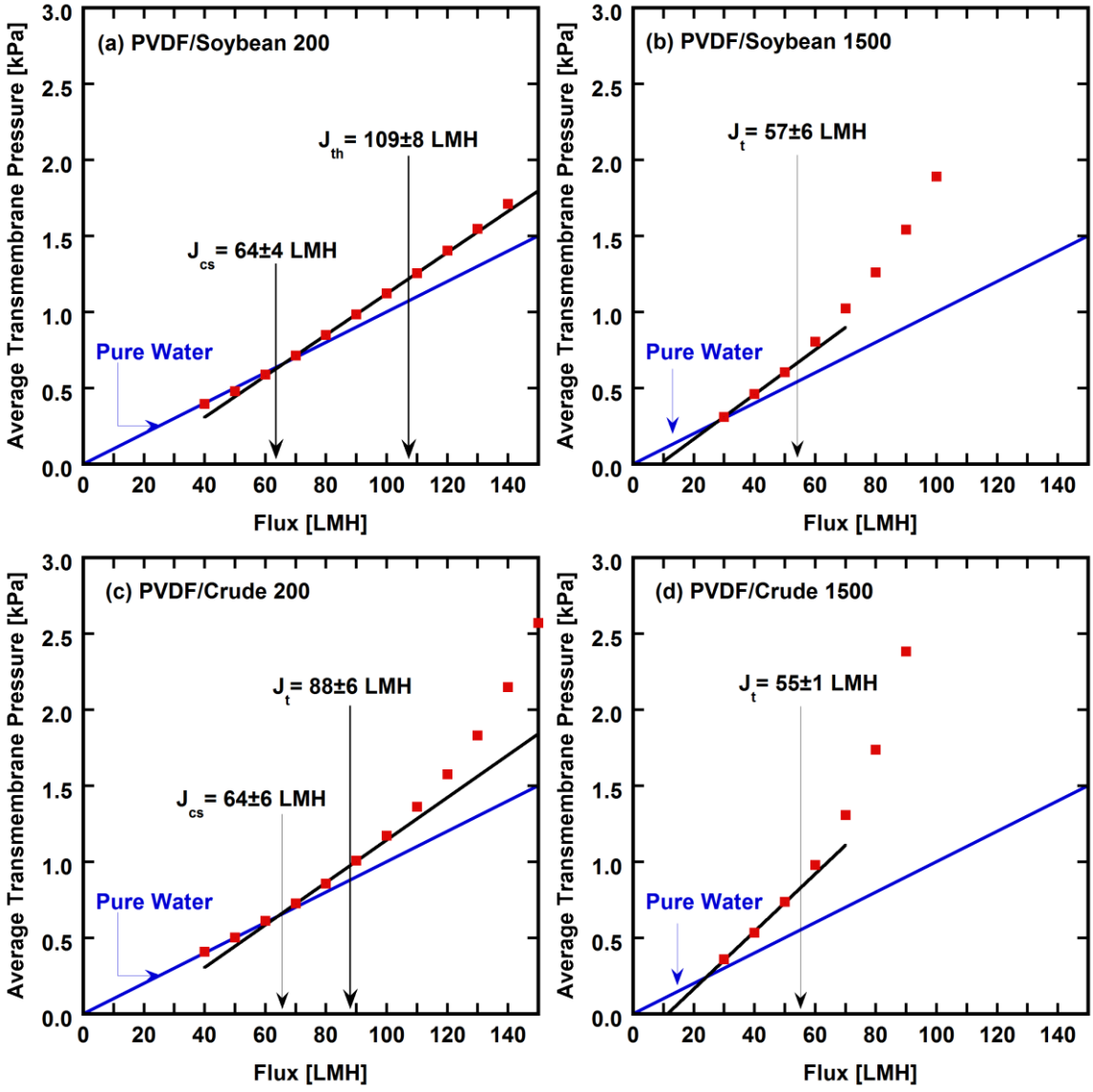

Figure 2. Estimated critical and threshold fluxes for PVDF MF membranes with various oil emulsions. Feed flow rate =2 L/min (feed flow velocity = 43 cm/s, Re ≈ 2500). Figures (a) and (c) are reproduced from a previous publication [10].

Table 1. Estimated critical and threshold fluxes and R_B values for each membrane-oil emulsion combination.

Membrane	Emulsion	Critical Flux [LMH]	Threshold Flux [LMH]	R_B [m^{-1}]
PVDF MF	Soybean 200 [10]	64±6	104±8	5.2×10^9
	Soybean 1500	-	57±6	5.91×10^9
	Crude 200 [10]	64±4	88±6	5.6×10^9
	Crude 1500	-	55±1	6.96×10^9
PS UF [5]	Soybean 1500	12	62	9.3×10^{11}

4.2 Membrane fouling below the critical flux

The PVDF MF membrane was challenged with 200 ppm oil emulsions in a constant flux crossflow fouling test. The permeate flux was maintained at 50 LMH, which was below their critical fluxes. TMP and resistance profiles are shown in Figure 3. TMP remained constant throughout the experiment. The mass transfer resistance was equal to that of a clean membrane, also indicating that no fouling occurred at this flux.

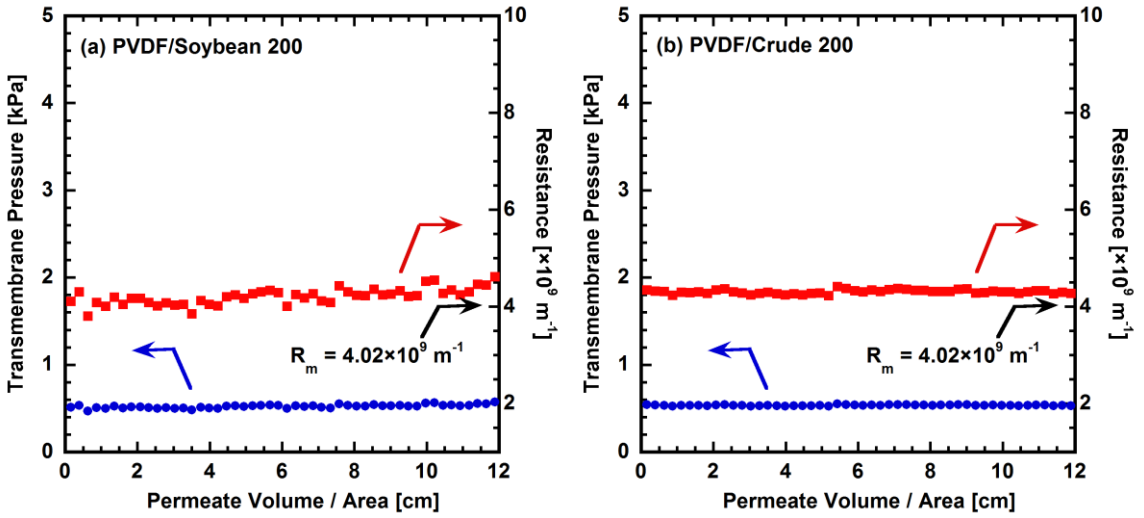

Figure 3. TMP and resistance profiles of a PVDF MF membrane in a constant flux operation below the critical flux. Feed flow rate = 2 L/min (feed flow velocity = 43 cm/s, Re ≈ 2500). The permeate flux was 50 LMH, which was below the critical flux (i.e., 64 LMH). R_m is the clean membrane resistance.

4.3 Membrane fouling below the threshold flux

4.3.1 PVDF MF membrane fouling below the threshold flux

The PVDF MF membrane was challenged with 1500 ppm oil emulsions in constant flux crossflow fouling tests. The flux was maintained at 50 LMH, which was below their threshold flux values. TMP and resistance profiles are shown in Figure 4. The initial resistance was equal to that of a clean membrane. The resistance increased at the beginning of an experiment and then reached a steady state. Interestingly, the steady state resistance coincided with R_B values calculated from flux-stepping experiments (cf.,

Table 1). A similar constant long-term resistance was observed in literature reports [13], although the reported resistance was not compared with flux-stepping experiments.

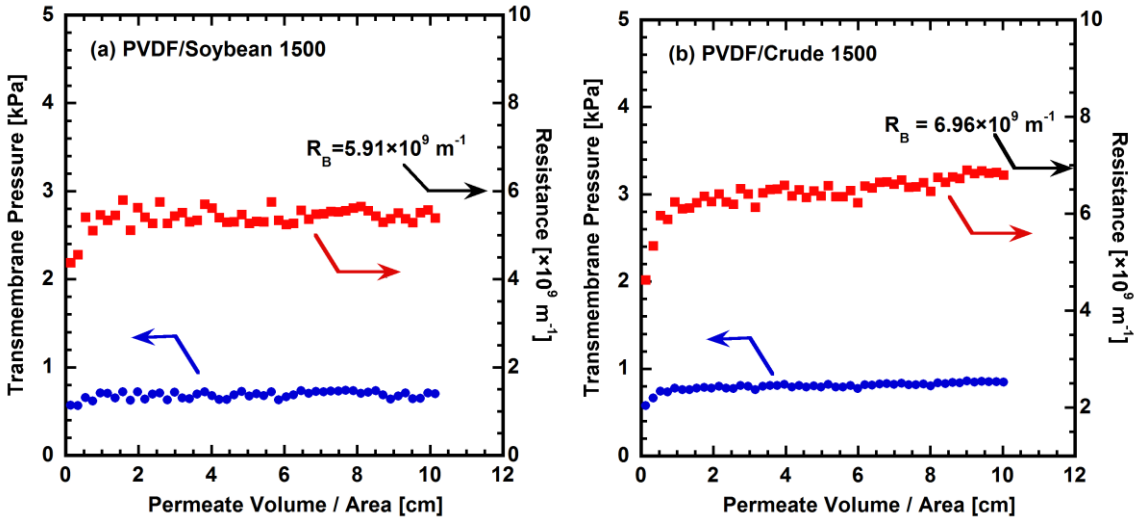

Figure 4. TMP and resistance profiles of a PVDF MF membrane in a constant flux operation below the threshold flux. Feed flow rate = 2 L/min (feed flow velocity = 43 cm/s, Re ≈ 2500). The permeate flux was 50 LMH, which was below their threshold flux values. R_B is the mass transfer resistance corresponding to the slope of Line B in the TMP_{avg} -flux relationship.

4.3.2 PS UF membrane fouling below the threshold flux

Results shown in this section were adapted from an earlier publication [5]. The PS UF membrane was challenged with a soybean oil-in-water emulsion in both constant TMP and constant flux operations. The PS UF membrane had a relatively large clean membrane resistance to allow constant TMP tests to operate at initial fluxes below its threshold flux, which was not possible with the PVDF MF membrane. Three initial

fluxes, 25, 40, and 55 LMH, were selected to investigate the effect of initial flux, J_0, on fouling behavior below the threshold flux (i.e., 62 LMH).

Flux profiles for constant TMP operations and TMP profiles for constant flux operations are shown in Figure 5 (a) and (b), respectively. Decreases in permeate flux and increases in TMP occurred in the beginning of crossflow fouling tests. All six operations reached a steady state within 60 minutes. To compare the two operations, mass transfer resistance was plotted with respect to cumulative permeate volume per unit membrane area, as shown in Figure 5 (c). The R_B value (i.e., 9.3×10^{11} m^{-1}) is also shown in Figure 5 (c). Similar to the PVDF MF membrane (cf., Figure 4), the steady state resistance approached R_B. The steady state resistance was consistent regardless of the initial permeate flux and the operational mode. A unified resistance profile suggests that the fouling mechanism was the same in these operations. At fluxes below the threshold flux, membrane fouling was flux-driven, yet it was flux-independent.

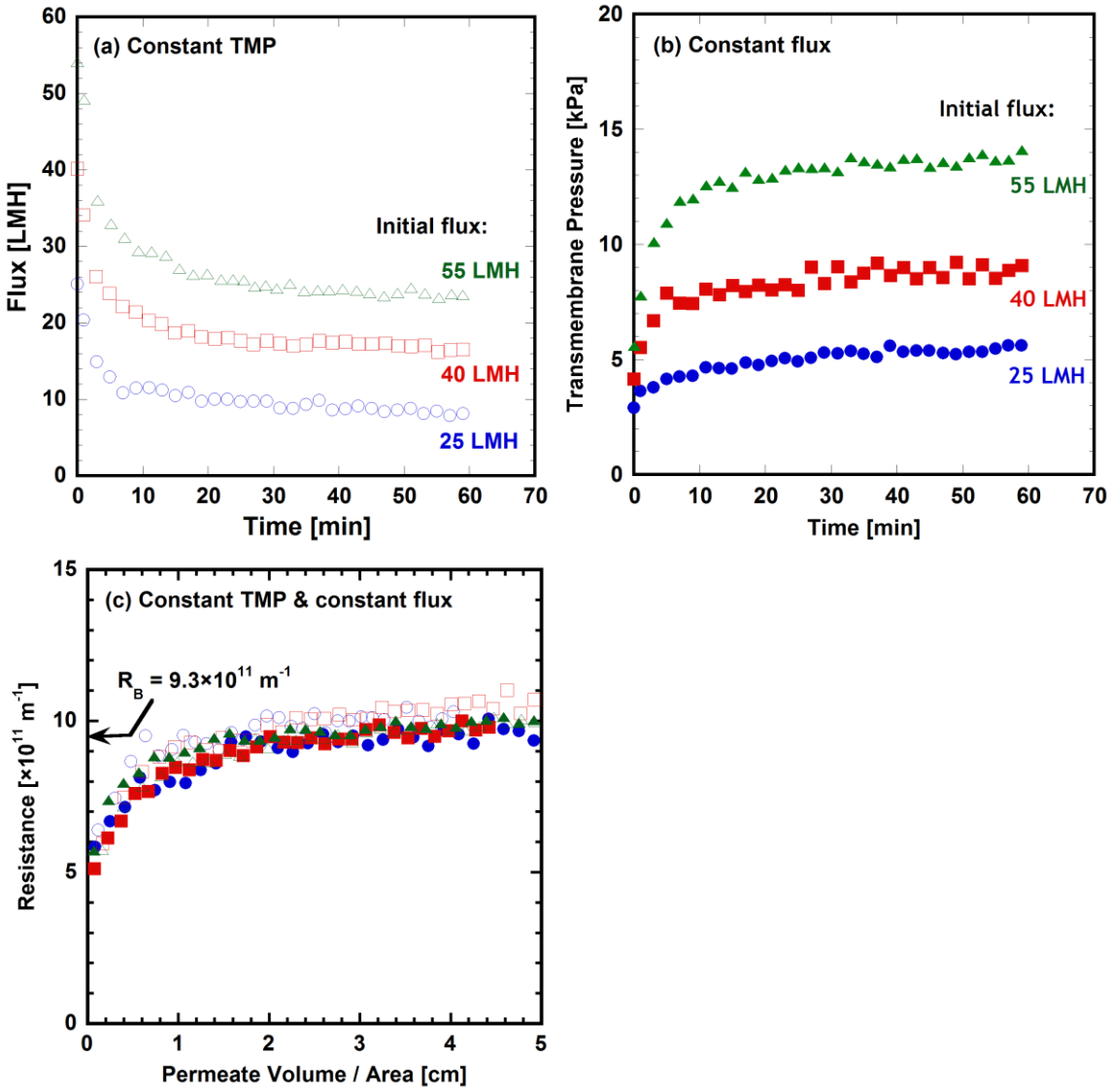

Figure 5. Fouling behavior of a PS UF membrane below the threshold flux. (a) Flux profiles for constant TMP operations. (b) TMP profiles for constant flux operations. (c) Resistance for all constant TMP and constant flux operations shown in (a) and (b). ○, □, and △ are constant TMP operations with $J_0 = 25, 40, 55$ LMH, respectively. ●, ■, and ▲ are constant flux operations with $J_0 = 25, 40, 55$ LMH, respectively. Feed flow rate = 0.8 L/min (feed flow velocity = 18 cm/s, Re ≈ 1000). Figure adapted from an earlier publication [5].

4.3.3 Fouling mechanisms below the threshold flux

In accordance with the threshold flux concept, as well as based on observations with the PVDF MF and the PS UF membrane, we postulated a unifying resistance profile for constant TMP and constant flux operations below the threshold flux, as illustrated in Figure 6 (c). The mass transfer resistance approaches a steady state resistance that can be predicted by flux-stepping experiments. In this limit, constant TMP and constant flux operations are comparable. In constant TMP operations below the threshold flux, permeate flux decreases initially and then approaches a steady state, as shown in Figure 6 (a). In constant flux operations below the threshold flux, TMP increases at the beginning of the operation and approaches a steady state, as shown in Figure 6 (b).

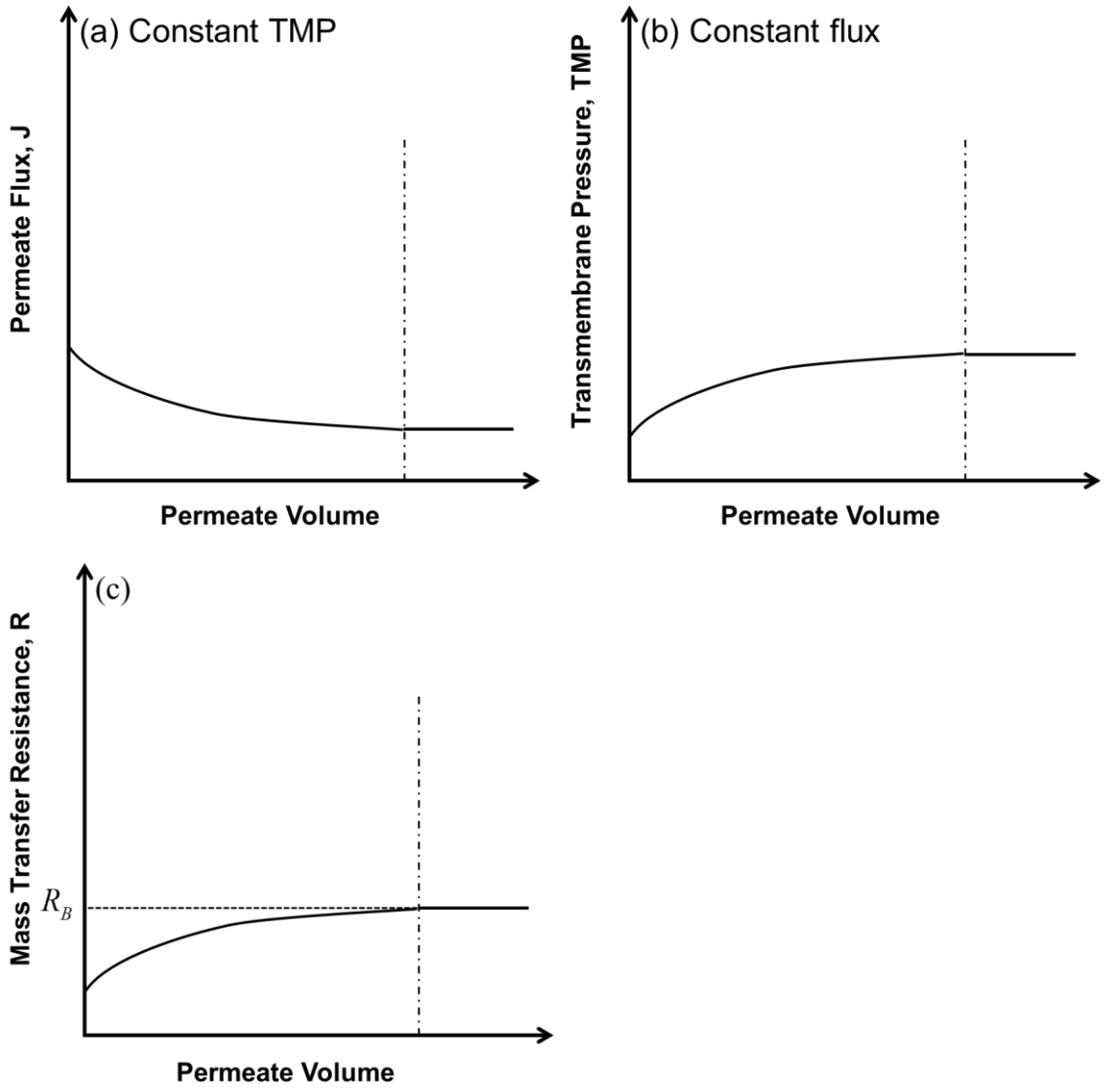

Figure 6. Illustrations of crossflow fouling tests (a) flux profiles for constant TMP operations, (b) TMP profiles for constant flux operations. (c) a unifying mass transfer resistance profiles for both constant TMP and constant flux operations. The initial permeate flux is lower than the threshold flux.

4.4 Membrane fouling above the threshold flux

4.4.1 PVDF MF membrane fouling above the threshold flux

The PVDF MF membrane was challenged with soybean 1500, crude 200 and crude 1500 emulsions in constant flux operations at 150 LMH, which was above their threshold fluxes. Figure 7 shows the TMP profiles for soybean 1500, crude 200 and crude 1500 emulsions. When challenged with the soybean 1500 and crude 200 emulsions, TMP increased relatively gradually until it entered a rapid "TMP jump" regime, followed by a pseudo-steady state. For the crude 1500 emulsion, the TMP evolution entered the TMP jump regime at the beginning of the experiment, indicating severe fouling. The upturn curve of the TMP profile later shifted to a similar pseudo-steady state. The crude 200 emulsion led to a higher pseudo-steady state TMP than that of the crude 1500 emulsion due to its higher critical pressure. The pseudo-steady state TMP will be discussed in detail later.

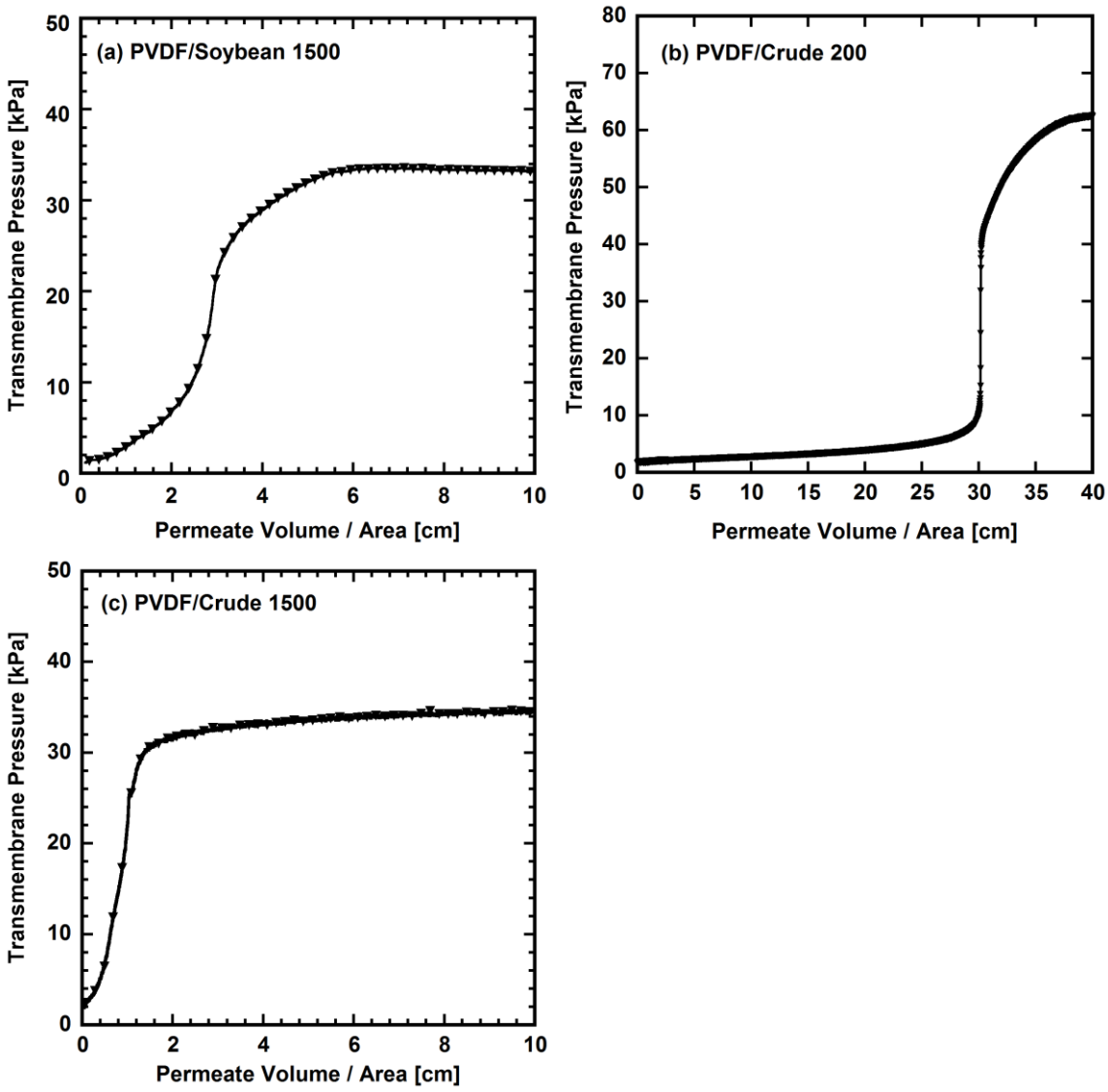

Figure 7. TMP profiles of a PVDF MF membrane in constant flux operations above the threshold flux. Feed flow rate = 2 L/min (feed flow velocity = 43 cm/s, Re $\approx$ 2500). The permeate flux was 150 LMH, which was above the threshold flux values.

4.4.2 TMP jump

In constant flux operations, TMP is a measure for the extent of fouling, while the slope of a TMP profile indicates the rate of fouling. An upwards curvature, such as the TMP jump, reflects the self-accelerating feature of constant flux operations. In constant flux operations, the overall permeate flux is maintained at a fixed value. The local flux, on the other hand, must increase to compensate for lessened open pores and a more restricted porous structure. An increased local flux can bring more foulant to the remaining pores and cause an increased rate of fouling. The TMP jump indicates severe fouling and the onset of cake/gel layer formation [5, 11]. The TMP jump phenomenon has been observed in long-term membrane bioreactor (MBR) studies [14-17], as well as constant flux colloidal fouling tests [18].

4.4.3 Critical pressure

The pseudo-steady state following the TMP jump is rarely reported [14, 15, 17-19]. In our study, the pseudo-steady state TMP corresponded with the critical pressure of an oil layer. Interfacial tensions and contact angles used in critical pressure calculation are reported in Table 2. The PVDF MF membrane pore diameter ranged from 0.27 to 0.45 μm, with a mean diameter of 0.32 μm. Membrane pore size distribution is shown in the Supporting Information.

Table 2. Interfacial tension and contact angle values for each membrane-foulant combination.

Membrane	Emulsion	Aqueous Phase	Contact Angle	$\gamma_{O/W}$ [mN/m]
PVDF MF	Soybean 200	Xiameter 20 ppm	121.4±3.6º	7.18±0.95
	Soybean 1500	Xiameter 150 ppm	62.8±4.0 º	4.94±0.93
	Crude 200	Triton 40 ppm	50.6±3.0º	8.74±0.24
	Crude 1500	Triton 300 ppm	47.4±4.0º	3.40±0.29
PS UF	Soybean 1500	Xiameter 150 ppm	46.7±2.5º	4.94±0.93

The critical pressure was calculated using Equations [2] and [3]. Figure 8 plots critical pressure as a function of membrane pore diameter. The relevant membrane pore size (i.e., 0.27 to 0.45 μm in diameter) was highlighted. The estimated critical pressure of oil droplets increased with increasing oil droplet diameter, indicating smaller oil droplets can enter the membrane porous structure more easily than bigger droplets, as shown in Figure 8 (a). The critical pressure of an oil layer was estimated to be 20 - 40 kPa for the crude 1500 emulsion. For a 0.32 μm diameter pore (i.e., the mean pore diameter), the critical pressure was 30 kPa. The pseudo-steady state TMP was approximately 34 kPa, which corresponds to a pore diameter of 0.29 μm. The diameter of the remaining pores at pseudo-steady state may have been restricted due to internal fouling. Figure 8 (b) shows oil layer critical pressure for soybean 1500, crude 200 and crude 1500 emulsions. For the three emulsions, the pseudo-steady state TMP corresponded with their respective critical pressures. The soybean 200 emulsion returned a negative critical pressure due to its large contact angle (or affinity) with the PVDF membrane. Oil droplets in the soybean 200 emulsion can readily penetrate through the PVDF membrane, therefore it would have

been impossible to form an oil layer. The PS UF membrane and soybean 1500 emulsion combination returned a critical pressure of approximately 3000 kPa. This critical pressure was beyond our instrument's pressure limit, therefore a pseudo-steady state TMP was not observed [5].

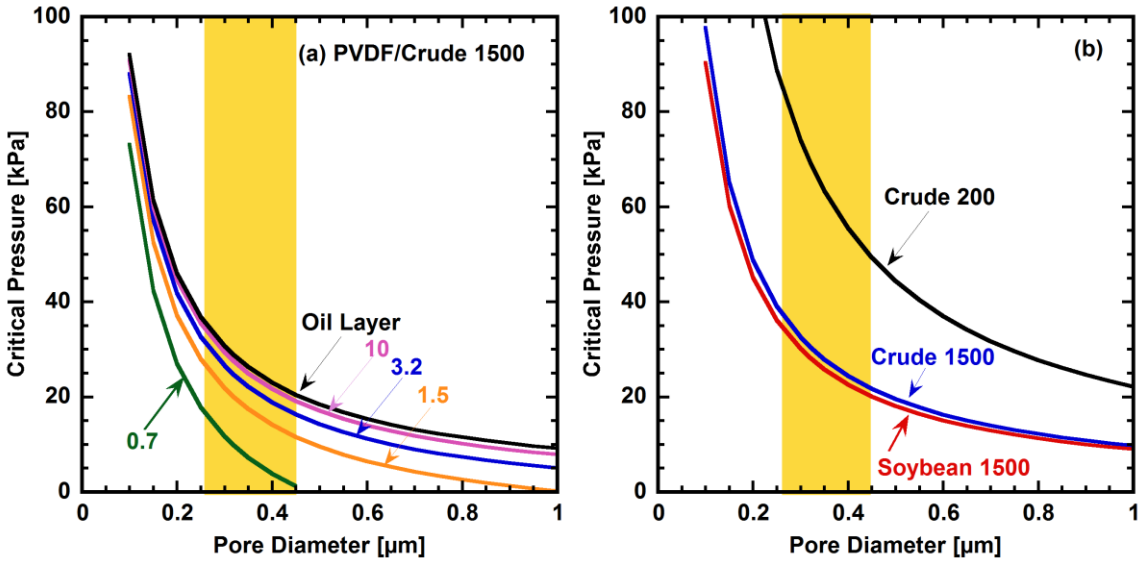

Figure 8. Critical pressure of various oil emulsions as a function of membrane pore diameter. (a) Oil droplets and oil layer critical pressures for the crude 1500 emulsion. The values shown in the figure are oil droplet diameters. (b) Oil layer critical pressures for soybean 1500, crude 200 and crude 1500 emulsions. The highlighted area is the relevant membrane pore size (i.e., 0.27 to 0.45 μm in diameter).

The critical pressure, which is unique for each membrane-foulant combination, served as an upper limit for TMP. The PVDF MF membrane was challenged with the crude 1500 emulsion at three different fluxes, all of which were above its threshold flux. As shown in Figure 9, the pseudo-steady state TMP was practically indifferent, which further supported that the critical pressure was the upper limit for TMP. This

correspondence between the critical pressure and the pseudo-steady state TMP indirectly supports that an oil layer was formed on the membrane surface. In the pseudo-steady state regime, oil deposition was in equilibrium with oil passage under the pseudo-steady state TMP, such that the oil layer was in a dynamic equilibrium.

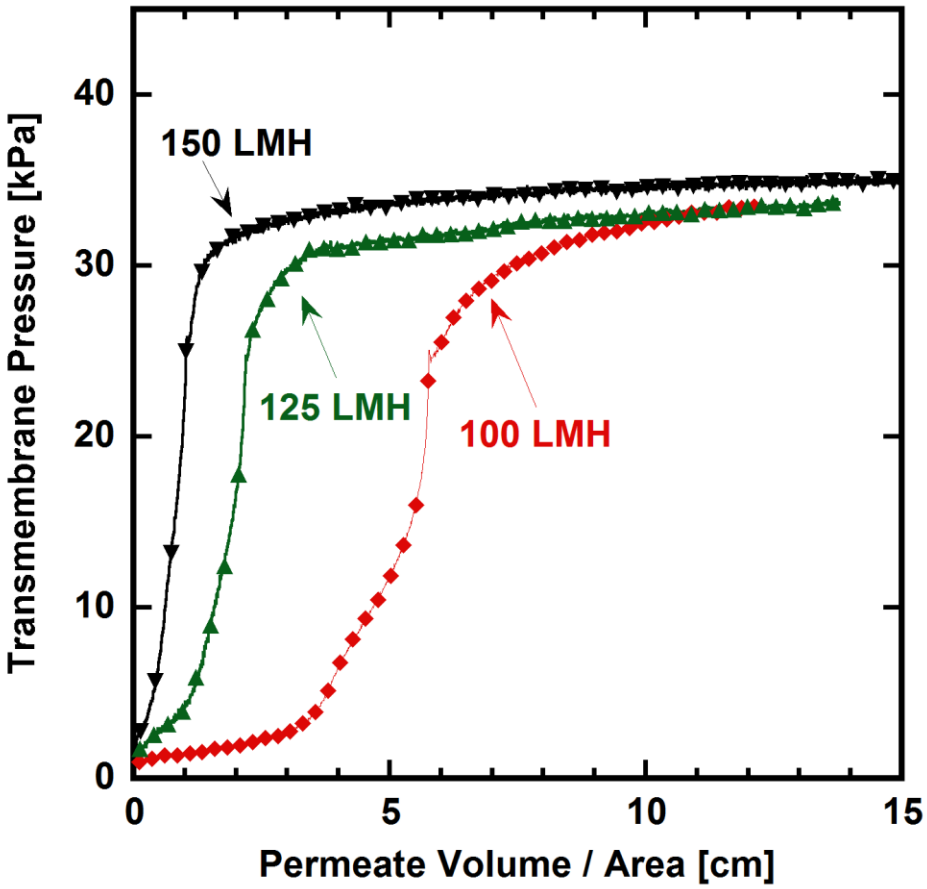

Figure 9. TMP profiles of a PVDF MF membrane in constant flux crossflow fouling tests above the threshold flux. Feed flow rate = 2 L/,min (feed flow velocity = 43 cm/s, Re ≈ 2500). The permeate fluxes were 100, 125 and 150 LMH. The pseudo-steady state TMP corresponded to the critical pressure for all three tests.

4.4.4 Fouling profiles for crossflow tests above threshold flux

We hypothesize that in constant flux operations above the threshold flux fouling develops in three stages. Figure 10 (a) and (b) illustrate TMP and resistance profiles, respectively, for a constant flux operation above the threshold flux. In constant flux operations, the TMP develops in three stages. TMP gradually increases in Stage I. The sharp TMP jump takes place in Stage II. Cake/gel layer starts forming in Stage II. As the cake/gel layer reaches its equilibrium, TMP enters a pseudo-steady state and corresponds to the critical pressure of an oil layer. With permeate flux being a fixed value, R is directly proportional to TMP, as shown in Figure 10 (b).

In some cases, the TMP profile may appear different from that shown in Figure 10 (a). If the fouling is severe enough that a slow fouling regime cannot be established, TMP may enter the TMP jump stage at the beginning of a fouling experiment, such as that shown in Figure 7 (c). The marked increase in TMP may breach the operating limit, so TMP is rarely allowed to develop freely. The three-stage TMP profile may not always be observed if the critical pressure is beyond the operating limit or an experiment is terminated before the TMP was fully developed. In cases where the critical pressure is a negative value, such as the soybean 200 emulsion in this study, TMP can increase continuously without an upper limit.

A three-stage flux profile was proposed for constant TMP operations [20]. With the development of critical and threshold fluxes, it becomes clear that this three-stage flux profile assumed a J_0 that was above the threshold flux, which caused the initial sharp decrease in flux. This high initial flux assumption is true for most constant TMP operations, nevertheless. Figure 10 (c) and (d) were adapted from literature to illustrate flux and resistance profiles for a constant TMP operation with an initial flux above the

threshold flux [20]. In Stage I, the permeate flux first experiences a sharp decrease. The rate of fouling (i.e., the slope of the flux profile) is the highest at the beginning of an experiment because the permeate flux is at its maximum at the beginning. In Stage II, the flux declines gradually because the rate of fouling decreases as the flux decreases. In Stage III, the flux reaches a "limiting flux" and the rate of fouling is net zero. With the TMP being a fixed value, R is inversely proportional to J. Unlike operations below the threshold flux, the two operational modes are not comparable due to the differences in local hydrodynamics.

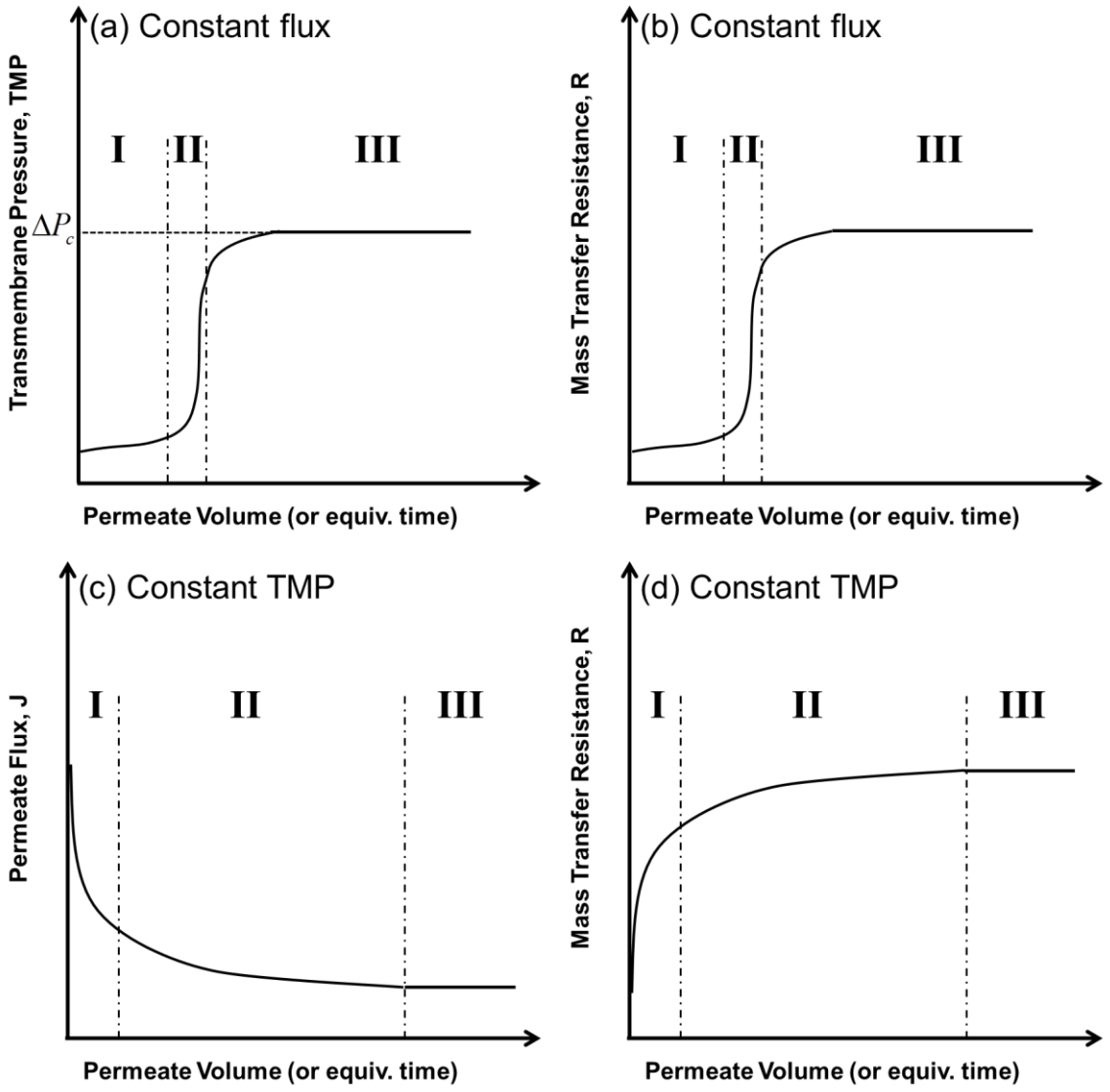

Figure 10. Illustrations of crossflow fouling tests (a) TMP profiles for constant flux operations, (b) Resistance profiles for constant flux operations. (c) Flux profiles for constant TMP operations and (d) Resistance profile for constant TMP operations. The initial permeate flux is above the threshold flux.

5. CONCLUSIONS

In this study, the effect of permeate flux on membrane fouling behavior was investigated. Critical and threshold fluxes were first determined using the flux-stepping technique. Constant flux crossflow fouling tests were performed at selected fluxes below and above the critical and threshold fluxes. Below the threshold flux, membrane fouling behavior was comparable in constant TMP and constant flux operations. The mass transfer resistance can be predicted by the slope of the TMP_{avg} -flux relationship from flux-stepping experiments. Membrane fouling in operations below the threshold flux was induced by the filtration, yet mass transfer resistance was independent of the imposed permeate flux. Above the threshold flux, the TMP profile for constant flux operations developed in three stages, an initial gradual TMP increase, followed by a TMP jump, and then approached a pseudo-steady state. The pseudo-steady state TMP corresponded to the critical pressure of an oil layer.

6. ACKNOWLEDGMENTS

The authors gratefully acknowledge financial support from Pall Corporation, James Fair Process Science and Technology Center at The University of Texas at Austin, the National Science Foundation (NSF) Center for Layered Polymeric Systems (DMR-0423914), and NSF Grant CBET 1160069. We would also like to thank American Refining Group for providing the crude oil.

7. REFERENCES

[1] R.W. Field, D. Wu, J.A. Howell, B.B. Gupta, Critical flux concept for microfiltration fouling. Journal of Membrane Science, 100 (1995) 259-272.

[2] R.W. Field, G.K. Pearce, Critical, sustainable and threshold fluxes for membrane filtration with water industry applications. Advances in Colloid and Interface Science, 164 (2011) 38-44.
[3] L.N. Sim, Y. Ye, V. Chen, A.G. Fane, Comparison of MFI-UF constant pressure, MFI-UF constant flux and crossflow sampler-modified fouling index ultrafiltration (CFS-MFI_{uf}). Water Research, 45 (2011) 1639-1650.
[4] H.K. Vyas, R.J. Bennett, A.D. Marshall, Performance of crossflow microfiltration during constant transmembrane pressure and constant flux operations. International Dairy Journal, 12 (2002) 473-479.
[5] D.J. Miller, S. Kasemset, D.R. Paul, B.D. Freeman, Comparison of membrane fouling at constant flux and constant transmembrane pressure conditions. Journal of Membrane Science, 454 (2014) 505-515.
[6] I.W. Cumming, R.G. Holdich, I.D. Smith, The rejection of oil by microfiltration of a stabilised kerosene/water emulsion. Journal of Membrane Science, 169 (2000) 147-155.
[7] F.F. Nazzal, M.R. Wiesner, Microfiltration of oil-in-water emulsions. Water Environment Research, 68 (1996) 1187-1191.
[8] T. Darvishzadeh, V.V. Tarabara, N.V. Priezjev, Oil droplet behavior at a pore entrance in the presence of crossflow: Implications for microfiltration of oil–water dispersions. Journal of Membrane Science, 447 (2013) 442-451.
[9] E.N. Tummons, V.V. Tarabara, Jia W. Chew, A.G. Fane, Behavior of oil droplets at the membrane surface during crossflow microfiltration of oil–water emulsions. Journal of Membrane Science, 500 (2016) 211-224.
[10] Z. He, D.J. Miller, S. Kasemset, L. Wang, D.R. Paul, B.D. Freeman, Fouling propensity of a poly(vinylidene) fluoride microfiltration membrane to several model oil/water emulsions. Manuscript in preparation.
[11] D.J. Miller, D.R. Paul, B.D. Freeman, A crossflow filtration system for constant permeate flux membrane fouling characterization. Review of Scientific Instruments, 84 (2013) 035003-035011.
[12] G.N. Lewis, R.T. Macdonald, The Viscosity of H^2H^2O. Journal of the American Chemical Society, 55 (1933) 4730-4731.
[13] J. Luo, L. Ding, Y. Wan, M.Y. Jaffrin, Threshold flux for shear-enhanced nanofiltration: Experimental observation in dairy wastewater treatment. Journal of Membrane Science, 409–410 (2012) 276-284.
[14] T.-N.-P. Nguyen, Y.-C. Su, J.R. Pan, C. Huang, Comparison of membrane foulants occurred under different sub-critical flux conditions in a membrane bioreactor (MBR). Bioresource Technology, 166 (2014) 389-394.
[15] D. Gao, Y. Fu, N. Ren, Tracing biofouling to the structure of the microbial community and its metabolic products: A study of the three-stage MBR process. Water Research, 47 (2013) 6680-6690.
[16] P. Le Clech, B. Jefferson, I.S. Chang, S.J. Judd, Critical flux determination by the flux-step method in a submerged membrane bioreactor. Journal of Membrane Science, 227 (2003) 81-93.

[17] J.S. Zhang, J.T. Zhou, Y.-C. Su, A.G. Fane, Transient performance of MBR with flux enhancing polymer addition. Separation Science and Technology, 45 (2010) 982-992.
[18] S.T.V. Sim, T.H. Chong, W.B. Krantz, A.G. Fane, Monitoring of colloidal fouling and its associated metastability using Ultrasonic Time Domain Reflectometry. Journal of Membrane Science, 401–402 (2012) 241-253.
[19] Q.-F. Liu, S.-H. Kim, S. Lee, Prediction of microfiltration membrane fouling using artificial neural network models. Separation and Purification Technology, 70 (2009) 96-102.
[20] L. Song, Flux decline in crossflow microfiltration and ultrafiltration: mechanisms and modeling of membrane fouling. Journal of Membrane Science, 139 (1998) 183-200.

Constant Permeate Flux Microfiltration of Oily Water

Supporting Information

Zhengwang He, Daniel J. Miller, Sirirat Kasemset, Donald R. Paul, Benny D. Freeman*

Department of Chemical Engineering, Center for Energy and Environmental Resources, and Texas Materials Institute, The University of Texas at Austin, 10100 Burnet Road Building 133, Austin, TX 78758

*Corresponding author (Tel: +1-512-232-2803; Email: freeman@che.utexas.edu)

Manuscript prepared for submission to *?*

1. EMULSION VISCOSITY

Emulsion viscosity was measured using an Anton Parr (Ashland, VA) MCR300 rheometer at 25ºC. Dynamic shear stress was measured in a shear rate range of 400 to 1600 s^{-1}. Table 1 presents measured emulsion viscosities in comparison with that of pure water [1, 2]. Emulsion viscosities were statistically the same as that of the pure water. Therefore, the permeate viscosity was assumed to be 8.95×10^{-4} Pa·s in resistance calculations.

Table 1. Emulsion viscosities.

Emulsion	Viscosity [$\times10^{-4}$ Pa·s]
Pure Water[2]	8.95
Soybean 200	8.75±0.40
Soybean 1500	8.91±0.26
Crude 200	8.98±0.48
Crude 1500	9.11±0.26

2. FLUX STEPPING DATA

TMP and flux profiles for flux-stepping experiments are presented in Figure 1.

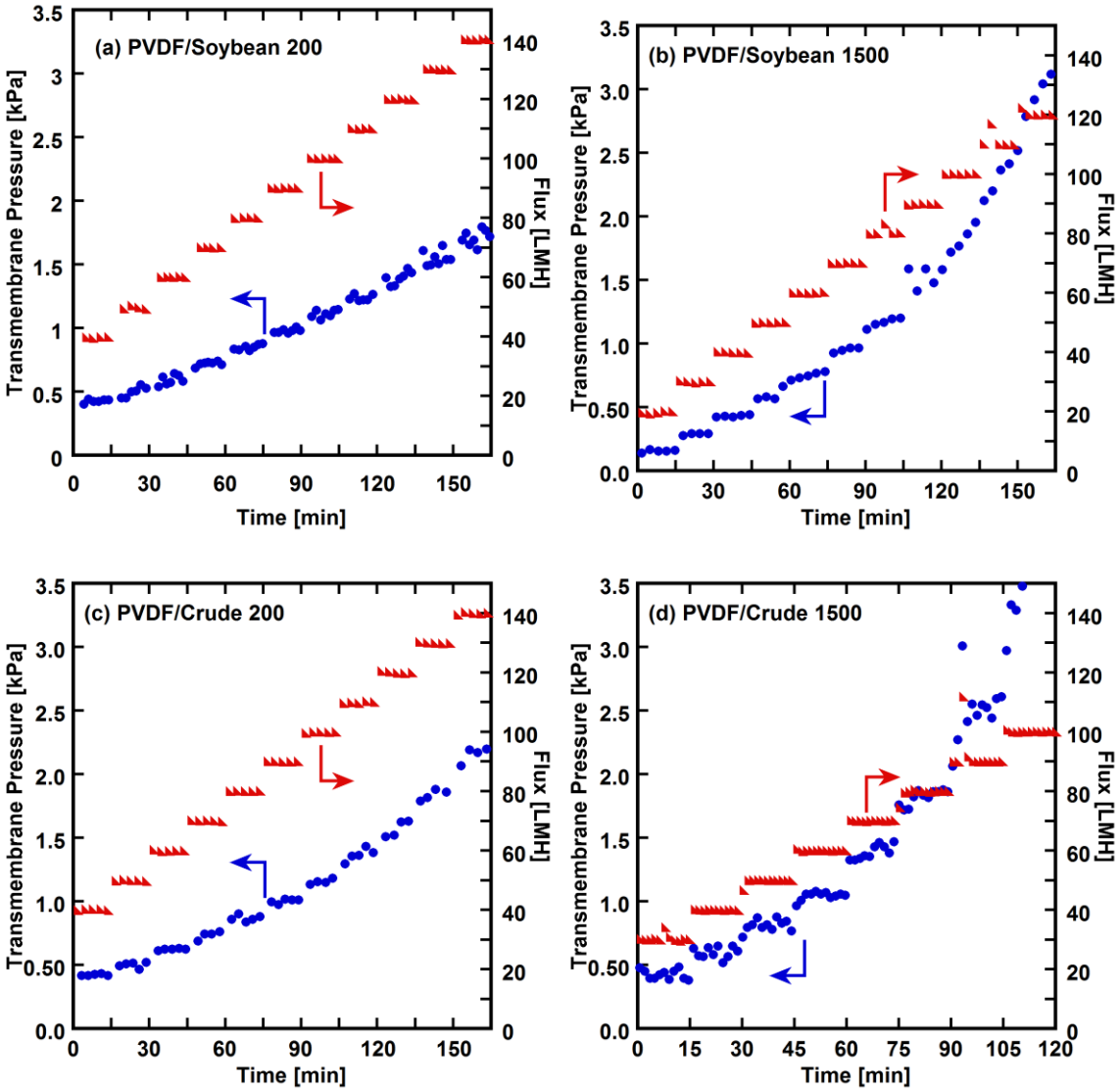

Figure 1. Flux stepping TMP and flux profiles for each membrane-foulant pair. Feed flow rate = 2 L/min. Flux was increased every 15 minutes by 10 LMH.

3. MEMBRANE PORE SIZE DISTRIBUTION

Membrane pore size was characterized with a Quantachrome Porometer 3G. Membrane pore size distribution is shown in Figure 2.

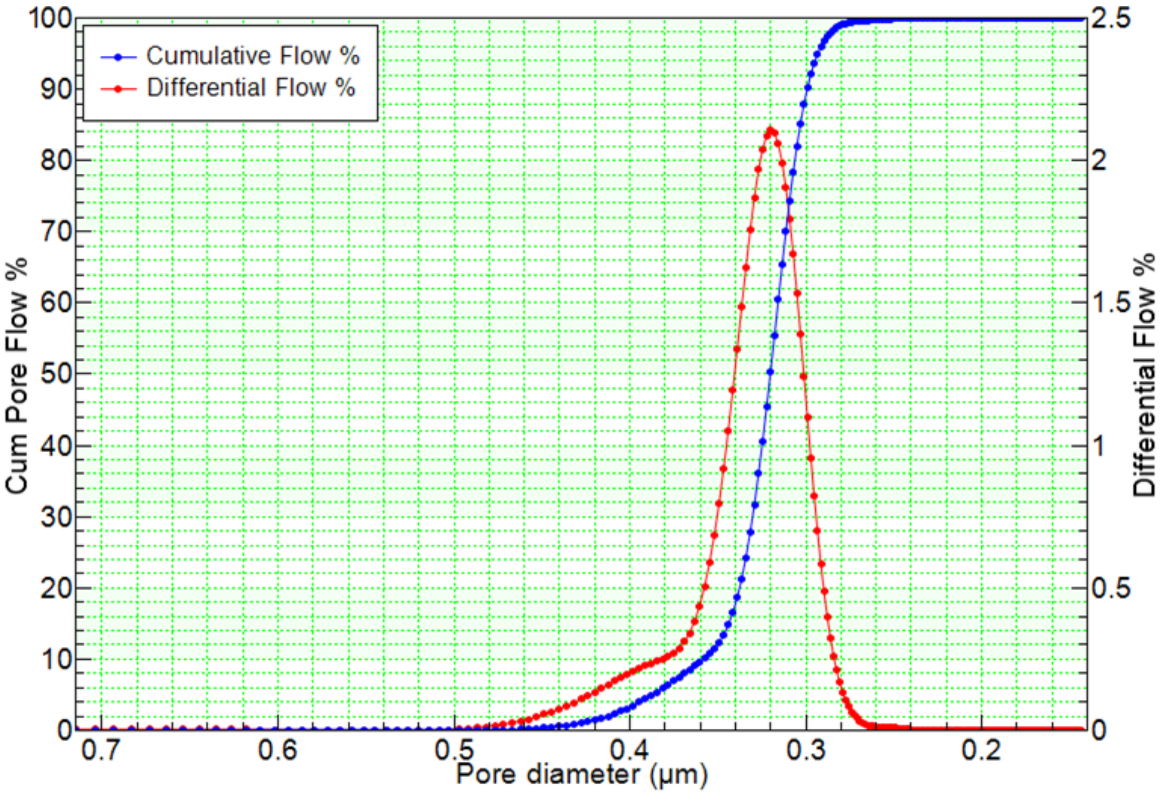

Figure 2. Membrane pore size distribution.

4. REFERENCES

[1] D.J. Miller, S. Kasemset, D.R. Paul, B.D. Freeman, Comparison of membrane fouling at constant flux and constant transmembrane pressure conditions. Journal of Membrane Science, 454 (2014) 505-515.
[2] G.N. Lewis, R.T. Macdonald, The Viscosity of H^2H^2O. Journal of the American Chemical Society, 55 (1933) 4730-4731.
[3] Z. He, D.J. Miller, S. Kasemset, L. Wang, D.R. Paul, B.D. Freeman, Fouling propensity of a poly(vinylidene) fluoride microfiltration membrane to several model oil/water emulsions. Manuscript in preparation.
[4] H.J. Busscher, J. Arends, Determination of the surface forces γ_s^d and γ_s^P from contact angle measurements on polymers and dental enamel. Journal of Colloid and Interface Science, 81 (1981) 75-79.
[5] M. Stressmann, C. Moresoli, Effect of pore size, shear rate, and harvest time during the constant permeate flux microfiltration of CHO cell culture supernatant. Biotechnology Progress, 24 (2008) 890-897.
[6] X. Sun, D.M. Kanani, R. Ghosh, Characterization and theoretical analysis of protein fouling of cellulose acetate membrane during constant flux dead-end microfiltration. Journal of Membrane Science, 320 (2008) 372-380.